Hindawi
Advances in Civil Engineering
Volume 2022, Article ID 1769739, 13 pages
https://doi.org/10.1155/2022/1769739

Research Article

Optimal Evaluation of the Rheological Parameters for STF Dampers in Semi-Rigid Joints of Steel Structures Using Response Surface Method

Ruby Freya [1] **and R. Senthil** [2]

[1]*Department of Civil Engineering, Sri Venkateswara College of Engineering, Sriperumbudur, India*
[2]*Department of Civil Engineering, Anna University, Chennai, India*

Correspondence should be addressed to Ruby Freya; ruby.freya@gmail.com

Received 27 August 2022; Revised 19 November 2022; Accepted 2 December 2022; Published 31 December 2022

Academic Editor: Agathoklis Giaralis

This work deals with the multiobjective optimization of rheolohical parameters on a novel designed flexible joints using shear thickening fluid dampers (STFD) on steel structures. The proposed damper consists of the shear thickening fluid (STF) with the combination of nano-silica and PEG (400) sonicated to achieve colloidal dispersion of nanoparticles. Series of cyclic loading were imposed on the frames equipped with STF dampers to assess their impacts on T-steel frames. The stiffener end plate is bolted over the corner of the joints that are subjected to bending moment. The multi-objective optimization using the response surface method of the rheological parameters for STF dampers was studied in order to reduce the dynamic forces and moments produced in a semi-rigid joint of the steel structures. Results from the analysis were used to obtain correlations between the response variables and the input factors (effective stiffness of 449.89 N/mm, complex viscosity of 98.69 Pa.s, and damping constant of 446.99 N.s/mm) for the proposed STF damped semi-rigid joints.

1. Introduction

Steel structures are known for their high resilience towards deflection loads in comparison to concrete structures. These structures have found scope for fast track construction due to their pre-eminent charactertistics of ductility, strength to weight ratio, and easiness to dismantle. The integrity and serviceability of the steel frames against seismic disasters becomes a critical task for the structural engineers to design for maximum lateral stability [1]. When subjected to cyclic loads, the steel frame construction demonstrates appropriate deformation capability. Steel members with high stiffness are necessary for bearing wave impacts; however, steel's low intrinsic damping is a disadvantage for vibration suppression [2]. Design changes in the beam-to-column areas that maintain structural strength while increasing energy dissipation capability are critical. The brittle failure potential of steel constructions is considerably reduced by the greater deformation capability of semirigidity. Excessive deformation caused by less structural stiffness and insufficient energy dissipation in bolt connections remain problems when appropriate resistance to dynamic loads is needed.

A link between a beam and a column is subject to the effects of axial force, shearing force, bending moment, and torsion. Additionally, for the majority of connections, the axial and shearing deformations are often insignificant in contrast to the rotational deformation. Moment-rotational deformation behaviour of the connections for nearly all rotations is nonlinear and invariably irreversible. The value of rotation increases for the same moment in direct proportion to the connection's degree of flexibility. The moment transmitted between adjacent components for a given magnitude of rotation will be lower for a more flexible connection, on the other hand. As a connection gets more flexible, the ultimate moment capacity—or the maximum moment that a link can transmit—decreases. Passive energy

dissipation systems (dampers) have been suggested as a viable and economical technique to decrease dynamic stresses on structures in order to acquire the aforementioned connections. The basic function of these systems is to absorb or consume the majority of the energy input acquired from cyclic loads, decreasing the energy dissipation demand on primary structural elements (i.e., beams and columns in frame structures) and minimizing potential structural damage.

Buildings are routinely protected from earthquakes using fluid viscous dampers (FVDs). The ideal FVD design, placement, and size have been extensively studied over the previous four decades. This study provides a summary of the most popular methods from the substantial amount of research in the field [3].

When designing nonlinear building structures, both with and without passive dampers, earthquake loading must be taken into account. Since the start of the research in roughly 1980, numerous investigations have been conducted. An extensive analysis of the subject is provided in this article [4, 5].

Effective viscous damper design for elastic-plastic moment frames is suggested using the critical double impulse (DI) input velocity adjustment method. Both random ground vibrations and pulse-like near-fault ground motions can be handled by the recommended method [6].

Under resonant, long-lasting ground vibrations, high-rise buildings' resilience is assessed. The evaluation approach takes into account elements like lifelines and system redundancy in the building. Many investigations are provided for assessing the robustness of structures under a numerical model with multishocks [7].

Researchers investigated several types of dampers incorporated in steel constructions in order to determine the effective damping capacities in beam column joints.

Nonlinear viscous dampers can greatly improve system vibration isolation performance across a larger frequency range than linear dampers. High force-to-volume (HF2V) lead-based dampers were created by Rodgers et al. [8] to provide considerable resistive forces while preserving compact exterior dimensions.

A dual-pipe damper in the beam-to-column connection is found to be economical, simple to make, and simple to install. The reinforced concrete (RC) as first story frames with slit type dampers as rocking column enhances the connections ductility and moment carrying capacity. When comparing the ultimate energy dissipation capacity of slit-plate dampers in terms of the damage index ID, nonlinear time history studies were utilised to assess the energy dissipation demand on the dampers during strong earthquakes [9].

Ghaedi examined the use of metals' inelastic property, using metallic dampers, hysteric behaviour, and high energy absorption capacity [10]. The energy input from earthquakes can be dissipated very effectively through the inelastic deformation of metals. Devices that utilise this method of energy dispersion include metallic dampers [11].

STF (Shear thickening fluid) acts as an alternative to traditional materials that operates with external control for mitigitaing the structural vibrations which has the state of dynamic response to external excitations. (STF), a new smart material for energy dissipation, has been introduced [12].

Shear thickening formation is a typical phenomenon in suspended materials of the fluid that increases viscosity with the appiled shear rate. Controlling this tendency to thicken continues to be a major challenge, with empirical treatments ranging from altering particle surfaces and shapes to changing solvent properties [13]. But none of these methods permits modifying the flow properties while shearing [14]. Shear thickening was found to be efficiently eliminated by deliberately applying a high-frequency, low-amplitude shear perturbation orthogonal to the prevailing shearing flow. The viscosity of the suspension can be reduced by up to two decades on demand thanks to the orthogonal shear, which functions as a regulator in the suspension. We show in a different configuration that same effects may be produced simply by shaking the sample against the main shear direction. Overall, the ability to manipulate shear thickening in situ opens the door to designing materials with controllable mechanical properties [15, 16]. The current investigation focuses on the usage of STF damped semi-rigid joints in T frame connections subjected to cyclic loads.

2. Materials and Methods

2.1. Synthesis and Rheological Characterization of STF. The nano-silica employed to create the STF suspensions in this study has a relative density of 2.6 g/ml and principal particle pore sizes of 6–11 nm (SISCO Research labs, Mumbai, India). Ethylene glycol (PEG 400, $C_{2n}H_{4n+2}O_{n+1}$), the carrier fluid used in this experiment, has a hydroxyl value ranging from 265 to 295 mg KOH/g (Merck Specialties Private Limited, Maharashtra, India.). The nano-silica particles were ground using high energy ball mill at 2000 rpm for 13 hours to ensure uniformity in sieve particle size. Using an electronic scale, the nano-silica and carrier fluid (PEG 400) were precisely calculated and manufactured. In a beaker positioned in the centre of the agitator, the carrier fluid PEG 400 was created. The mixing speed of the agitator was set to 1000 rpm. The fumed nano-silica was progressively blended into the carrier fluid. The samples were shaken for 3 hours with an ultrasonicator to ensure that the particles were evenly distributed in the mixture. The STF samples were then vacuum-dried in a table furnace for 24 hours at 80°C. A shear viscometer was used to assess the rheological parameters of the STF. STF samples with a mass fraction of 20% underwent rheological tests (see Figure 1). In both static and dynamic loading scenarios, the STF rheology is evaluated using a parallel-plate rheometer (MCR 301, Anton Paar Companies, Germany). The parallel plate's diameter is 20 mm, and its thickness is 0.2 mm. At 25°C, the viscosity was determined. STF viscosity is measured using both ascending and descending loading.

2.1.1. Experimental Work. Through mechanical testing and simulation, the STFD was subjected to the cyclic loads (Type: MTS 793 series). The STFD was attached to the MTS on one

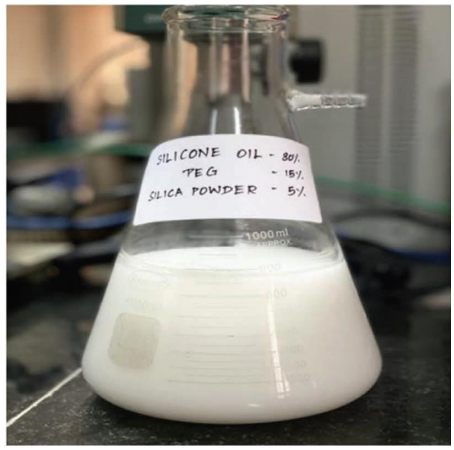

Figure 1: Ultrasonicated STF with 80% silicone oil, 15% PEG, and 5% silica powder.

end and to a frame attached to the response frame on the other. The schematic layout and a picture of the experimental machinery used for cyclic testing are shown in Figures 2 and 3, respectively. To investigate the behaviour of the STFD under various sinusoidal loading scenarios with a constant amplitude of 20 mm, several cyclic experiments were conducted. A 1000-hertz sample rate is used. Studying the STFD's characteristics at varied loading frequencies is the goal of the first set of loading examples. Eight separate loading frequencies were mandated (0.01, 0.1, 0.5, 1.0, 1.5, 2.0, 2.5, and 3.0 Hz). The dynamic performance of STFD will be examined under long-term loading situations with different loading frequencies in the second set of loading scenarios. There were three different loading frequency inputs employed in this investigation: 1.0, 2.0, and 3.0 Hz. 200 cycles were applied to each frequency. To ensure shear thickening performance recovery, a 3-hour gap was established between each loading. Verification tests (amplitude, 20 mm; loading frequency, 1 Hz) were run prior to each test to ensure that the STFD performance was restored.

2.1.2. Identification of Test Parameters for Rheological Characteristics. The rheological test parameters in semi-rigid STF damper joints in steel constructions are determined through their impact on the response characteristics during cyclic loading. Load frequency (Hz), percentage of STF with oil, initial viscosity (Pa.s), stiffener thickness (mm), and applied force were all evaluated (kN). In the response surface method, the aforementioned components are provided as input parameters (RSM). Table 1 lists the process parameters and operating range.

The response surface tool (RSM) is a mathematical and statistical method for issue analysis. By generating a regression model, this RSM approach reveals the relationship between rheological features and the impacting operating test factors. It was utilised to establish a link between the response variables and the input parameters. Since thermal spray is a cost-effective method, it is particularly good for reducing the cost of productivity in the coating process. A higher degree polynomial model was used to approximate the link between these variables. To approximate the link between the input and response variables, the suggested study employs a second-order polynomial function.

The proposed study employed a central composite design (CCD) and a second-order (quadratic) polynomial model for rheological properties to assess the effects of input factors on response values. Load frequency, initial viscosity, stiffener thickness, applied force, and % of STF with oil are the input variables in the response surface method. To acquire the effective complex viscosity and damping constant value on the proposed STF damper, the effective parameters contained in the design of experiments RSM were altered. During the optimization process, the response (resulting) variables' useful range was discovered. Table 2 shows the values of the tabulated responses.

3. Results and Discussion

3.1. ANOVA. The ANOVA (analysis of variance) approach was used to examine the variation among the parameter clusters. ANOVA was used to acquire rheological parameters, and the results are shown below. Table 3 lists the results for the complex viscosity.

The p value of the proposed model is found to be lesser than F value with 0.4440. Hence, the suggested model is found to be significant. The R^2 value is found to be 0.8761. This ensures that the data points were successfully fitted on the curve. The adjusted R^2 value is found to be 0.7522 which is lesser than the R^2 value. This gives the data line for regression equation.

The model is significant, as shown by the model F value of 7.07 in Table 3. Only 0.04% of the time will an F value this large occur due to noise. In cases when "Prob > F" is less than 0.0500, model terms are relevant. The model terms A, C, D, AD, A^2, B^2, C^2, and D^2 are essential in this situation. Values above 0.1000 suggest that the model terms are irrelevant.

According to Table 3, the model F value is 1.37, and the model is not significant when compared to the noise. Due to noise, a large F value has a 27.01% chance of happening. When "Prob > F" is smaller than 0.0500, model terms become important. In this circumstance, AD is a crucial model term. Values greater than 0.1000 suggest that the model terms are unimportant.

The $p$value of the proposed quadratic model with 0.8414 is found to be higher than Fvalue of 0.6485. Hence, the suggested model is found to be significant. The R^2 value is found to be 0.4318. This ensures that the data points were successfully fitted on the curve. The adjusted R^2 value is found to be 0.1162 which is lesser than the R^2 value. This gives the data line for regression equation.

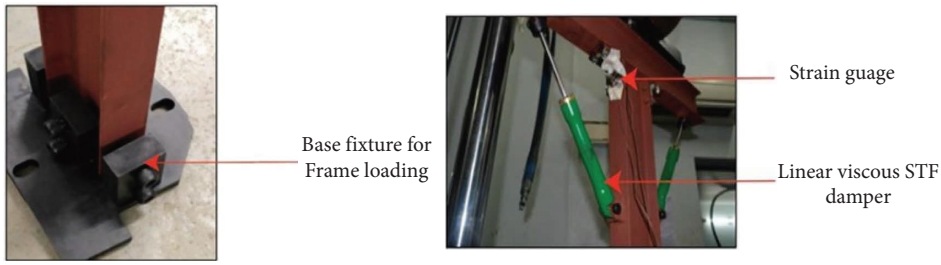

Figure 2: Photographic view of the base fixture and strain gauge over semi-rigid joints.

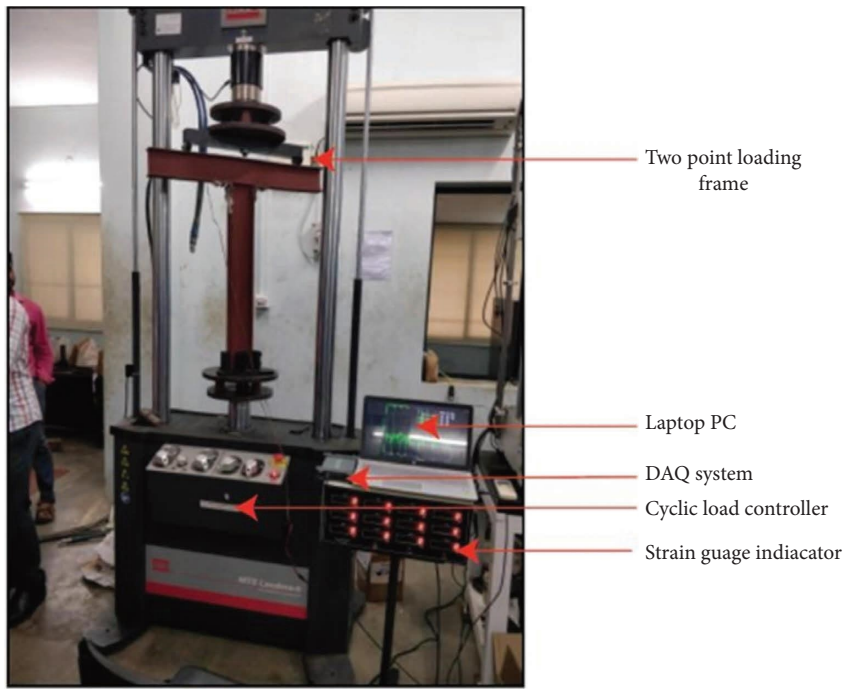

Figure 3: Photographic view of the experimental setup under cyclic loads.

Table 1: Process parameters and working range.

Factors	Level	Low level	High level
Load frequency (Hz)	1.75	0.8800	2.00
% of STF with oil	42.72	32.50	49.20
Initial viscosity (Pa.s)	39.56	32.00	50.00
Stiffener thickness (mm)	8.54	8.00	9.50
Applied force (kN)	96.77	60.00	120.00

Table 2: Response variables' resulting working range.

Variable	Range
Complex viscosity	65 Pa.s to 150 Pa.s
Damping constant	100 MN.s/m to 890 MN.s/m
Effective stiffness	350 N/mm to 550 N/mm

Table 3: Analysis of variance for complex viscosity.

Source	Sum of squares	df	Mean square	F value	p value	
Model	6698.75	20	334.94	0.6485	0.8414	Significant
A (load frequency)	57.90	1	57.90	0.1121	0.7402	
B (% of STF with oil)	27.69	1	27.69	0.0536	0.8185	
C (initial viscosity)	0.2347	1	0.2347	0.0005	0.9831	
D (stiffener thickness)	2.20	1	2.20	0.0043	0.9485	
E (applied force)	389.73	1	389.73	0.7546	0.3922	
AB	6.90	1	6.90	0.0134	0.9088	
AC	253.91	1	253.91	0.4916	0.4888	
AD	663.75	1	663.75	1.29	0.2662	
AE	15.88	1	15.88	0.0307	0.8620	
BC	1095.82	1	1095.82	2.12	0.1560	
BD	92.28	1	92.28	0.1787	0.6756	
BE	257.30	1	257.30	0.4982	0.4859	
CD	114.53	1	114.53	0.2218	0.6412	
CE	205.34	1	205.34	0.3976	0.5333	
DE	847.28	1	847.28	1.64	0.2104	
A^2	122.77	1	122.77	0.2377	0.6295	
B^2	483.81	1	483.81	0.9367	0.3411	
C^2	1658.96	1	1658.96	3.21	0.0835	
D^2	50.48	1	50.48	0.0977	0.7568	
E^2	26.98	1	26.98	0.0522	0.8208	
Residual	14978.40	29	516.50			
Lack of fit	11524.94	22	523.86	1.06	0.5046	Not significant
Pure error	3453.46	7	493.35			
Cor total	21677.15	49				

$$\begin{aligned}\text{Complex viscosity} = {} & 263.24 + 125.68 * \text{load frequency} - 1.66 * \%\text{ of STF with oil} + 6.21 * \text{initial viscosity} \\ & - 56.88 * \text{stiffener thickness} - 2.22 * \text{applied force} + 0.09 * \text{load frequency} * \%\text{ of STF with oil} \\ & - 0.55 * \text{load frequency} * \text{initial viscosity} - 10.84 * \text{load frequency} * \text{stiffener thickness} \\ & + 0.04 * \text{load frequency} * \text{applied force} - 0.07 * \%\text{ of STF with oil} * \text{initial viscosity} \\ & + 0.27 * \%\text{ of STF with oil} * \text{stiffener thickness} - 0.01 * \%\text{ of STF with oil} * \text{applied force} \\ & + 0.28 * \text{initial viscosity} * \text{stiffener thickness} + 0.22 * \text{stiffener thickness} * \text{applied force} \\ & - 4.73 * \text{loadfrequency}^2 + 1.69 * \text{stiffener thickness}^2.\end{aligned} \tag{1}$$

The model F value of 0.588 in Table 4 indicates that the model is significant. An F value this large might happen owing to noise only 0.01% of the time. When "Prob > F" values are less than 0.0500, model terms are likely to be important. A, B, C, and D are important model terms in this instance. The proposed model's p value is found to be less than F value with 0.0001. Thus, it is determined that the recommended model is important. The R^2 value is found to be 0.8675. This ensures that the data points were successfully fitted on the curve. The adjusted R^2 value is found to be 0.8455 which is lesser than the R^2 value. This gives the data line for regression equation.

Table 4: ANOVA for damping constant.

Source	Sum of squares	df	Mean square	F value	p value	
Model	$7.091E+05$	20	35454.06	0.5880	0.8899	Significant
A (load frequency)	4618.08	1	4618.08	0.0766	0.7839	
B (% of STF with oil)	748.21	1	748.21	0.0124	0.9121	
C (initial viscosity)	64429.08	1	64429.08	1.07	0.3098	
D (stiffener thickness)	205.11	1	205.11	0.0034	0.9539	
E (applied force)	89489.97	1	89489.97	1.48	0.2329	
AB	$1.242E+05$	1	$1.242E+05$	2.06	0.1619	
AC	98257.44	1	98257.44	1.63	0.2119	
AD	5671.13	1	5671.13	0.0941	0.7613	
AE	16128.08	1	16128.08	0.2675	0.6089	
BC	4787.31	1	4787.31	0.0794	0.7801	
BD	44357.31	1	44357.31	0.7357	0.3981	
BE	75991.51	1	75991.51	1.26	0.2708	
CD	273.78	1	273.78	0.0045	0.9467	
CE	32947.45	1	32947.45	0.5465	0.4657	
DE	52164.50	1	52164.50	0.8652	0.3600	
A^2	3851.28	1	3851.28	0.0639	0.8023	
B^2	19106.44	1	19106.44	0.3169	0.5778	
C^2	9405.06	1	9405.06	0.1560	0.6958	
D^2	5071.89	1	5071.89	0.0841	0.7739	
E^2	81879.64	1	81879.64	1.36	0.2534	
Residual	$1.748E+06$	29	60291.95			
Lack of fit	$1.318E+06$	22	59898.97	0.9735	0.5596	Not significant
Pure error	$4.307E+05$	7	61527.00			
Cor total	$2.458E+06$	49				

$$\begin{aligned}\mathrm{Cd\,(da\,mping\ constant)} = {} & -748.68 - 308.51 * \text{load frequency} + 35.78 * \%\ \text{of STF with oil} \\ & - 1.87 * \text{initial viscosity} + 76.35 * \text{stiffener thickness} + 11.50 * \text{applied force} \\ & + 13.32 * \text{load frequency} * \%\ \text{of STF with oil} - 10.99 * \text{load frequency} * \text{initial viscosity} \\ & + 31.69 * \text{load frequency} * \text{stiffener thickness} - 1.33 * \text{load frequency} * \text{applied force} \\ & - 0.16 * \%\ \text{of STF with oil} * \text{initial viscosity} - 5.94 * \%\ \text{of STF with oil} * \text{stiffener thickness} \\ & - 0.19 * \%\ \text{of STF with oil} * \text{applied force} - 0.43 * \text{initial viscosity} * \text{stiffener thickness} \\ & + 26.54 * \text{load frequency}^2 + 16.98 * \text{stiffener thickness}^2.\end{aligned} \tag{2}$$

The model F value of 0.6716 in Table 5 suggests that the model is significant. A p value of 0.8209 was observed. The probability value is greater than the F value to achieve the model significancy. The effective stiffness was dependent on the % of STF with oil with the maximum p value of 0.9754. This ensures that the shear resistance offered by the STF was higher with the increase in % of concentration. As with the increase in load frequency on the structure, the displacement of the STF damper would be lesser with the increase in resistance to shocks by the fluid [17].

3.2. Effect of Complex Viscosity on Rheological Parameters. The complex viscosity of the shear thickening fluid is defined as the resistance occurring during the flow with the function of angular frequency. The diagnostic graphs that follow compare predicted values to actual values (Figures 4(a)–4(c)). The complex viscosity is not affected by the load range. The low frequency is crucial in complex viscosity. Complex viscosity is 0.258 mg/m. To obtain this low complex viscosity, the operational parameters load frequency and % of STF with oil were both set to 2 m/s and 30%, respectively. Figure 4(b) depicts the Box–Cox plot, which describes the statistical intervals based on normality. In the transformation function, define the normalcy of the real set data. Data that are not normally distributed can be transformed into a normal distribution using the Box–Cox transformation. The Box–Cox transformation is denoted by Y^{λ} where λ is a value between −3 and 3. This approach is intended to determine the standard deviation that minimize the variation of input parameters that suggests the complex viscosity.

The % of STF concentration is also a crucial component in determining complex viscosity. The complex viscosity drops consistently as coating thickness increases. Figure 5(a) depicts the perturbation curve. The contour graph in Figure 5(b) depicts the relationship between the input variables in complex viscosity. Figure 5(c) compares the

Table 5: ANOVA for effective stiffness.

Source	Sum of squares	df	Mean square	F value	p value	
Model	86492.70	20	4324.63	0.6716	0.8209	Significant
A (load frequency)	12738.61	1	12738.61	1.98	0.1702	
B (% of STF with oil)	6.25	1	6.25	0.0010	0.9754	
C (initial viscosity)	1607.23	1	1607.23	0.2496	0.6211	
D (stiffener thickness)	7427.21	1	7427.21	1.15	0.2917	
E (applied force)	5564.66	1	5564.66	0.8641	0.3603	
AB	6469.53	1	6469.53	1.00	0.3245	
AC	3154.17	1	3154.17	0.4898	0.4896	
AD	3764.95	1	3764.95	0.5847	0.4507	
AE	6707.72	1	6707.72	1.04	0.3159	
BC	441.05	1	441.05	0.0685	0.7954	
BD	403.28	1	403.28	0.0626	0.8042	
BE	2471.05	1	2471.05	0.3837	0.5405	
CD	843.58	1	843.58	0.1310	0.7200	
CE	4687.54	1	4687.54	0.7279	0.4005	
DE	4491.15	1	4491.15	0.6974	0.4105	
A^2	2437.84	1	2437.84	0.3786	0.5432	
B^2	1921.93	1	1921.93	0.2985	0.5890	
C^2	13457.42	1	13457.42	2.09	0.1590	
D^2	1935.10	1	1935.10	0.3005	0.5878	
E^2	2596.50	1	2596.50	0.4032	0.5304	
Residual	$1.867E+05$	29	6439.62			
Lack of fit	$1.354E+05$	22	6152.28	0.8379	0.6531	Not significant
Pure error	51398.95	7	7342.71			
Cor total	$2.732E+05$	49				

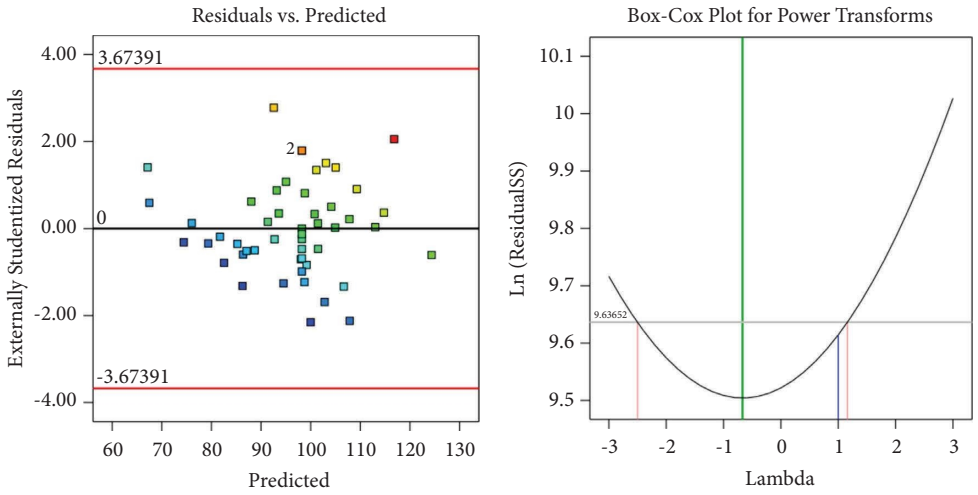

Figure 4: Continued.

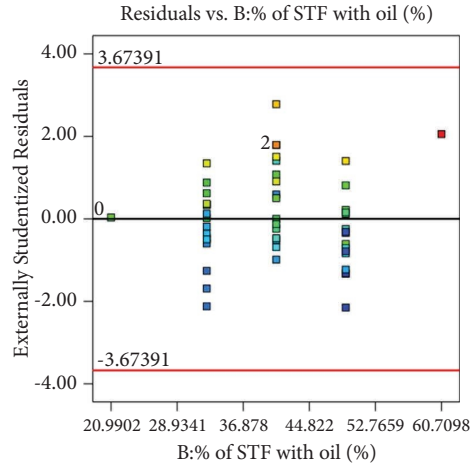

(c)

Figure 4: (a) Residuals vs. predicted values for complex viscosity. (b) Box–Cox plot for complex viscosity. (c) Residuals vs. process parameter for complex viscosity.

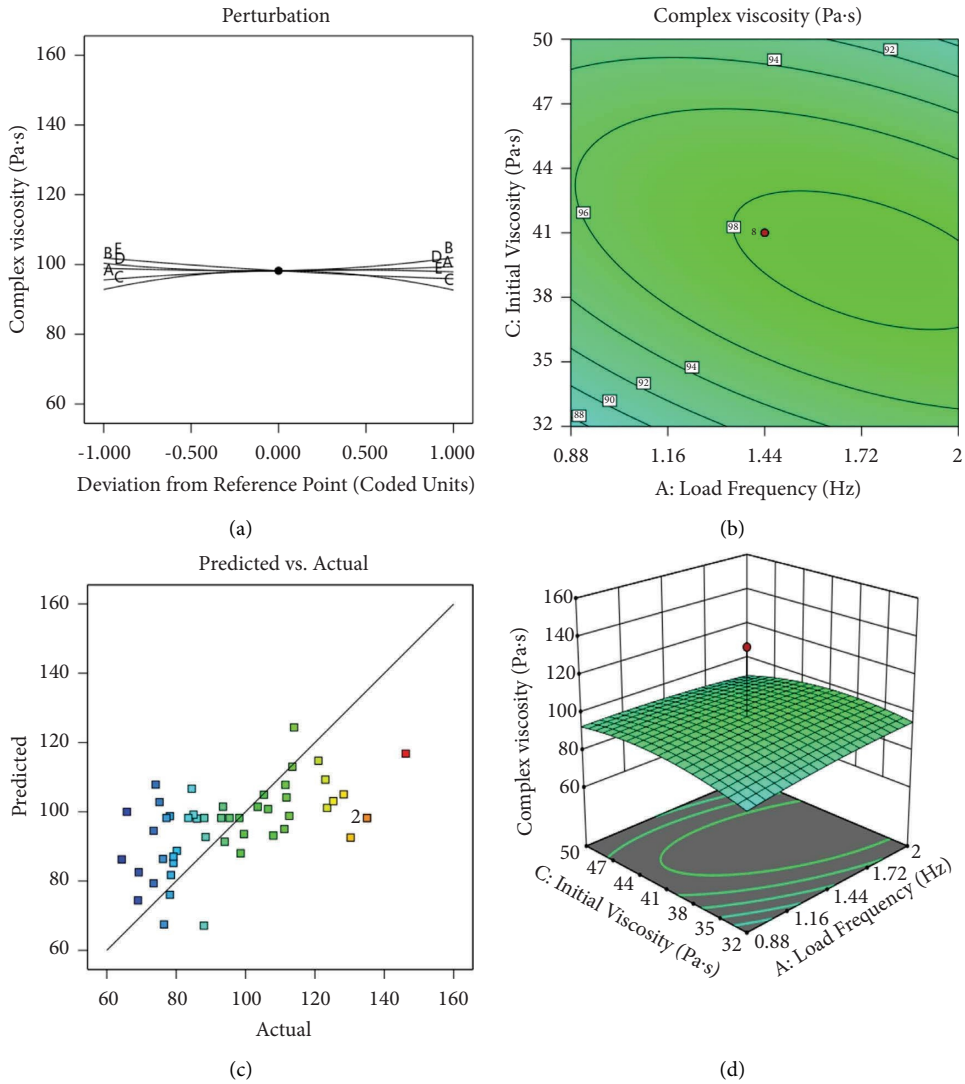

(a) (b) (c) (d)

Figure 5: (a) Perturbation for complex viscosity. (b) Contour graph for complex viscosity. (c) Predicted vs. actual values for complex viscosity. (d) 3D graph for complex viscosity.

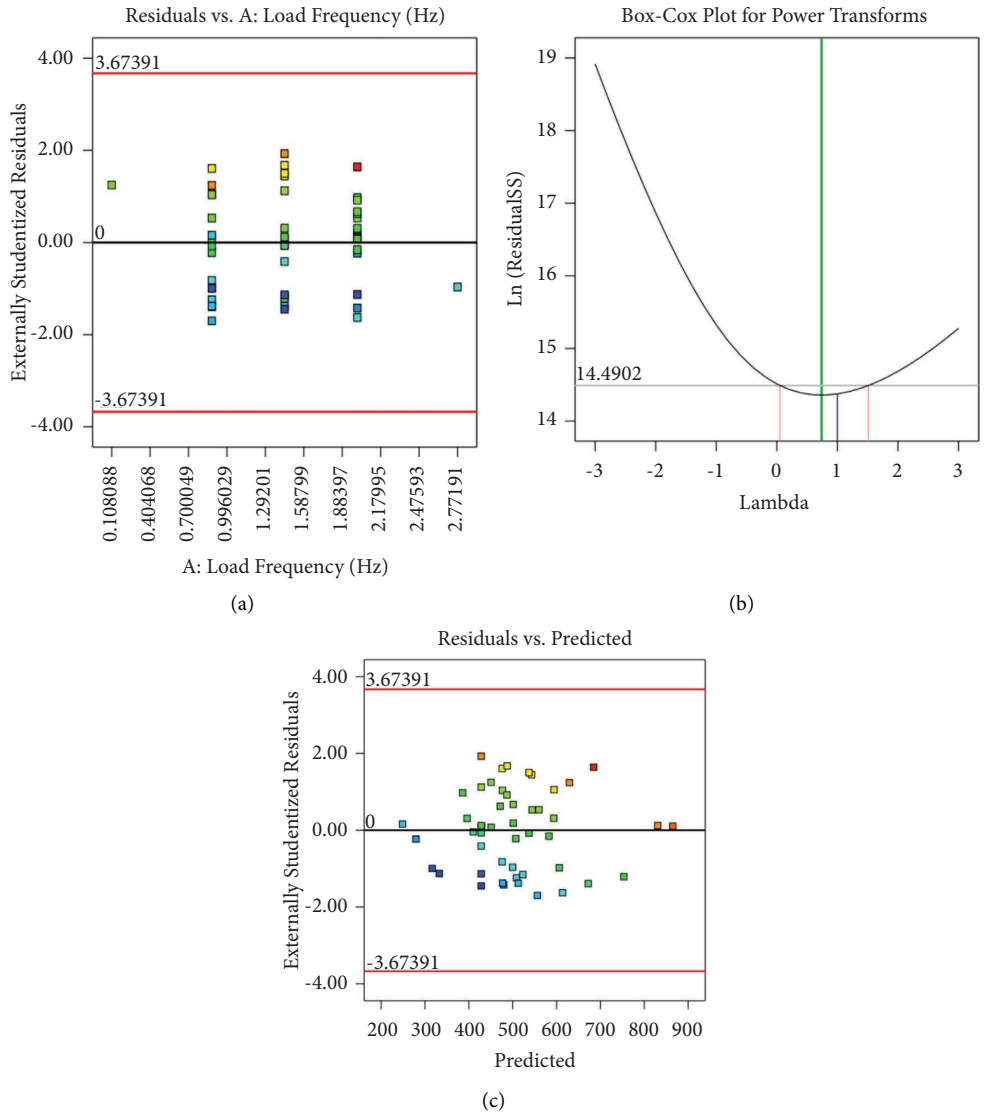

Figure 6: (a) Residuals vs. predicted values for damping constant. (b) Box–Cox plot for damping constant. (c) Residuals vs. process parameter for damping constant.

expected and real values. Figure 5(d) shows a 3D graph of complex viscosity with the input parameters.

3.2.1. Effect of Damping Constant on Operating Parameters. The frictional force caused by the STF travelling across the circumferential surface area of the peripheral layer has resulted in the creation of a damping constant. This damping constant represents the amount of weight lost within the pin's travelling surface area. The coating thickness has a significant impact on the damping constant with the hardened coated surface. The efficient concentration of STF is used to create the resistive hydrodynamic surface, which resists the damping constant. This hardness was attained by establishing a substrate layer on the area where the fracturing fluid travels [18]. The effective damping constant is 5.283 mg. Using the values for the input parameters indicated below, this effective value was achieved. The sliding speed was set at 2 m/s, and the coating thickness was preset at 300 m.

To achieve a low rate of damping constant, 0.175 kN was added to the applied pressure value. The % of STF concentration value was also raised to 20 to 30%. The relationship between the observed and real values is depicted by the diagnostics graph in Figures 6(a)–6(c). The Box–Cox plot graph (Figure 6(c)) depicts the power transformation process in relation to residual values.

The model graphs shown above (Figures 7(a)–7(d)) provide a clear perspective of the response value (damping constant) derived from the optimization procedure. The perturbation graph (Figure 7(a)) depicts the departure from the reference points as coded units with the damping constant. The 3D model clearly shows the optimization for damping constant (Figure 7(c)).

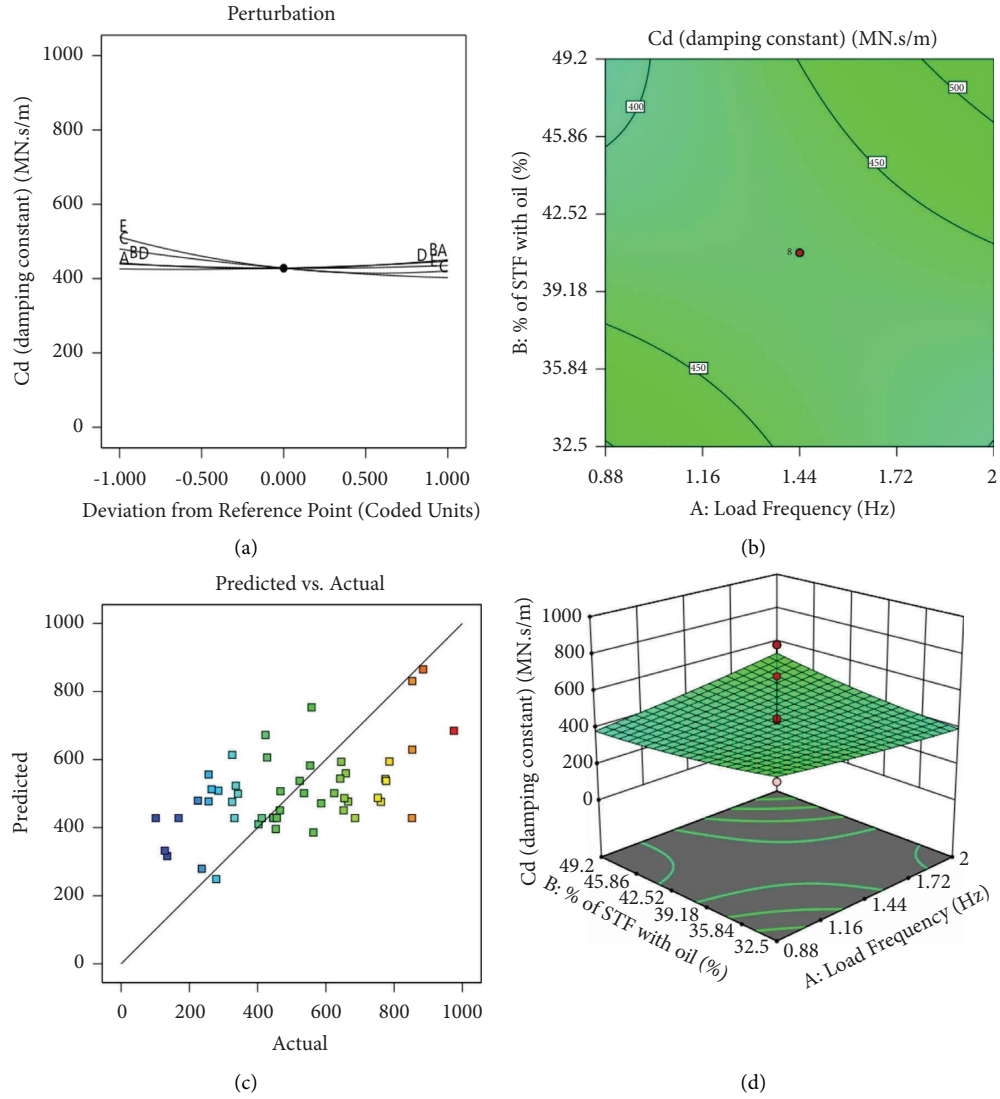

Figure 7: (a) Perturbation for damping constant. (b) Contour graph for damping constant. (c) Predicted vs. actual values for damping constant. (d) 3D graph for damping constant.

3.3. Effect of Effective Stiffness on Operating Parameters. The diagnostic graphs in Figures 8(a)–8(c) show the link between the residual and actual values. The power transformation values for this process are represented by the lambda value −1.87 in the Box–Cox plot (Figure 8(b)). The applied speed was related to the residual values. When the applied pressure falls below 0.2 kN, the coefficient of friction falls.

Effective stiffness and the input parameters are related, as shown by the contour graph in Figure 8(c) (applied pressure, sliding speed, coating thickness, and biolubricant). When the sliding speed is less than 5 m/s and the pressure range is less than 0.2 kN, the low coefficient of friction is reached. The coefficient of friction perturbation plot with respect to the symmetric convergence of the process parameters is shown in Figure 8(a). Figure 8(b) shows the Box–Cox plot. The strength against the complex viscosity created by the lubricant increases by obtaining the coefficient of friction value (μ) which is 0.076.

Reduced applied pressure lowers the frictional force between the moving surfaces and the fracturing fluid, resulting in a low coefficient of friction. Figure 9(d) depicts the effective coefficients of friction. The predicted and actual values were also compared (see Figure 9(b)). Figures 9(a) and 9(d) show the perturbation and the 3D graph representation, respectively.

3.3.1. Numerical Optimization. The points predicted using the response surface methodology's central composite design are presented in Table 1, and the impact on response variables was determined using this approach. The expected values of the response variables are also confirmed in Table 6 for comparison. With the help of these values, the complexity of the viscosity and damping constant of STF damped

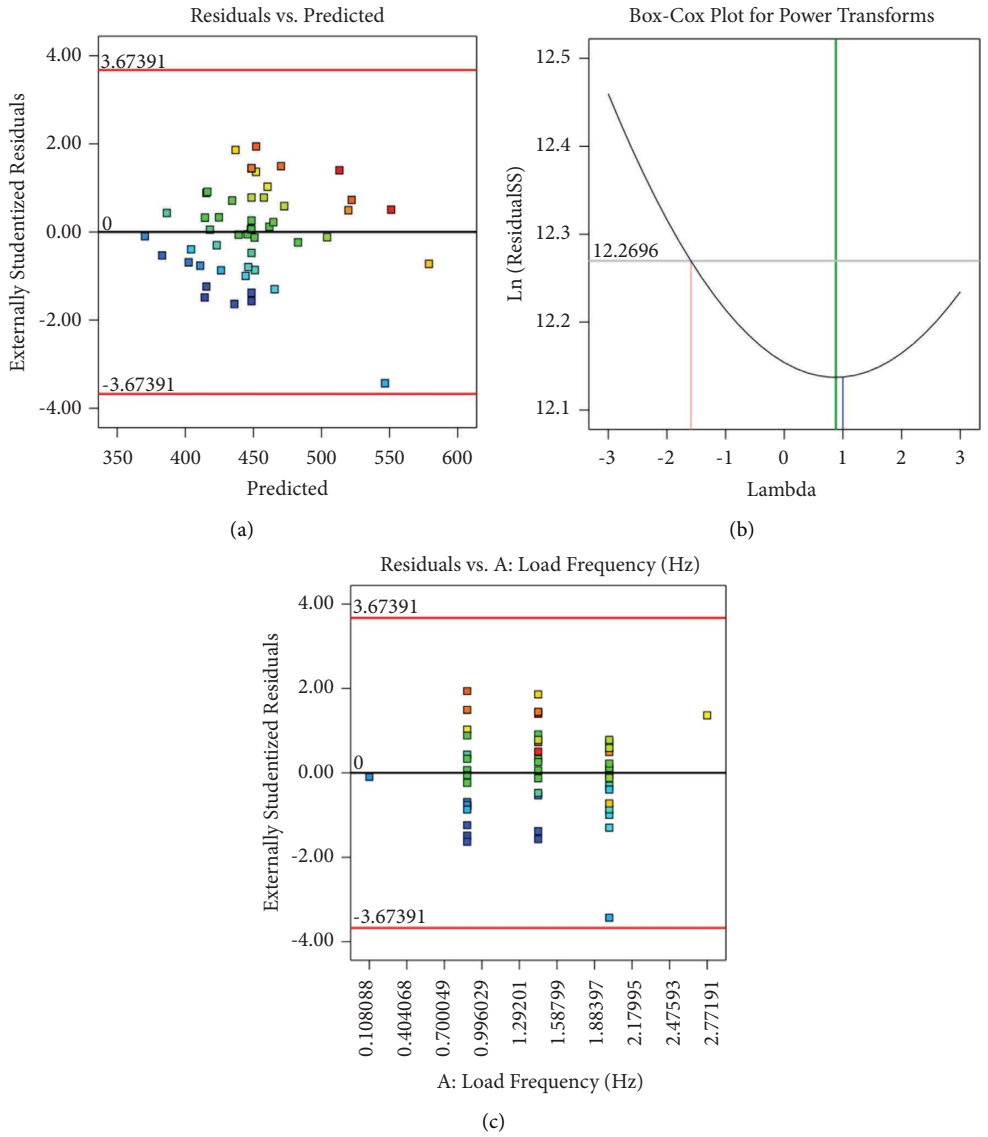

Figure 8: (a) Residuals vs. predicted values for effective stiffness. (b) Box–Cox plot for effective stiffness. (c) Residuals vs. process parameter for effective stiffness.

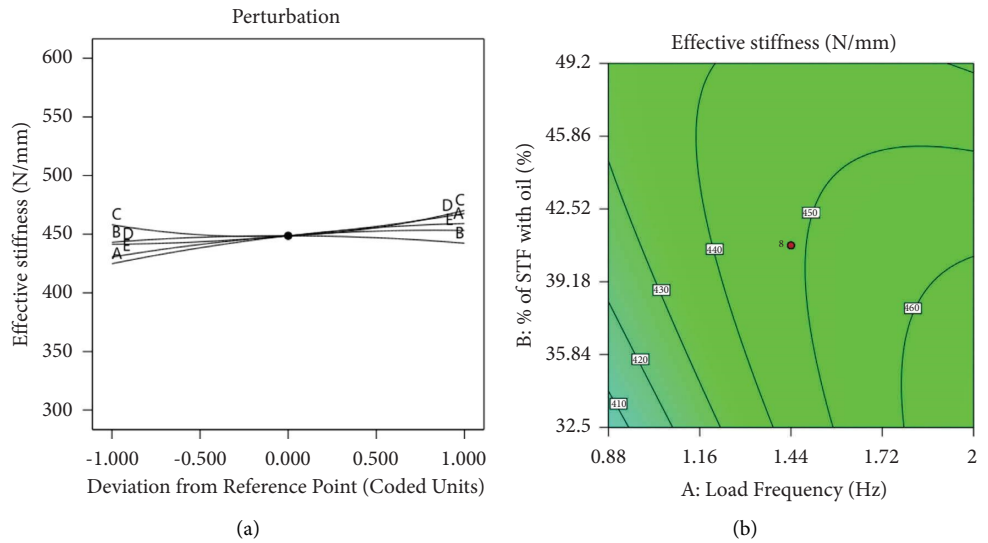

Figure 9: Continued.

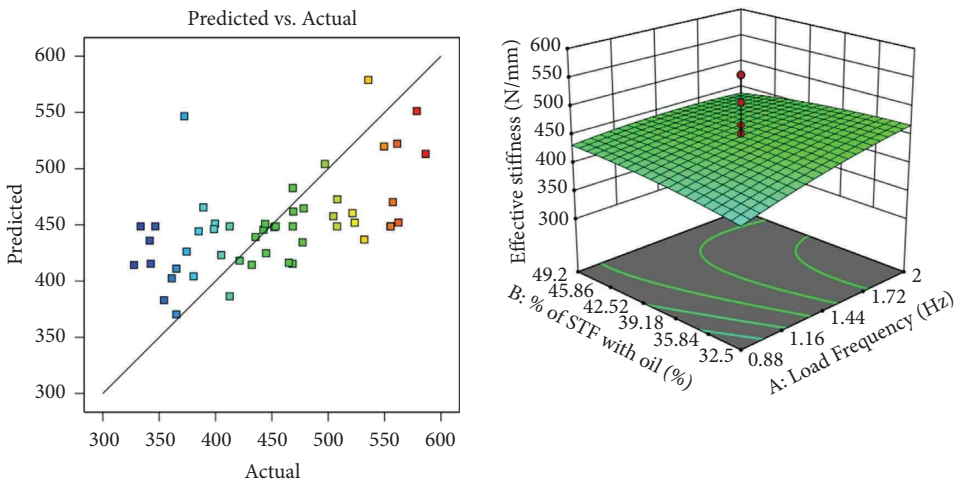

(c) (d)

Figure 9: (a) Perturbation for effective stiffness. (b) Contour graph for effective stiffness. (c) Predicted vs. actual values for effective stiffness. (d) 3D graph for effective stiffness.

Table 6: Point prediction of the response factors.

Response output	Predicted mean	Predicted median	Std dev	SE mean	95% CI low for mean	95% CI high for mean	95% TI low for 99% pop	95% TI high for 99% pop
Complex viscosity	98.6919	98.6919	22.7266	7.71753	82.9078	114.476	10.6652	186.719
Cd (damping constant)	446.995	446.995	245.544	83.3824	276.459	617.531	−504.07	1398.06
Effective stiffness	449.89	449.89	80.2473	27.2505	394.157	505.624	139.069	760.712

joints in steel constructions was reduced. The confirmation report table, as shown in Table 6, shows the measurement value for the response parameters or output characteristics.

When exposed to rapid stimuli, an STF, which is a highly concentrated colloidal suspension made up of monodisperse nanoparticles suspended in a carrying fluid, can exhibit both flowable and stiff behaviours [19]. In other words, the mechanical characteristics of the STF, such as its shear modulus and damping factor, can be modified. Additionally, STF may reverse both its energy absorption and deformation. STFs have a lot of potential for intelligent control in various engineering sectors because of these advantages [20]. The performance of an STF-filled damper under various ground acceleration situations was found to demonstrate a strong damping force at a greater peak ground acceleration while taking earthquake resistance into consideration. This suggests that the precise conditions needed by an STF to begin shear thickening behaviour can be provided by excitation loads present in civil engineering, such as those present near fault or during big earthquakes, which frequently involve substantial energy loads and fast-acting velocities.

4. Conclusion

The influence of complex viscosity and effective stiffness on the innovative STF damped semi-rigid joints was explored in this work utilising response surface methodology (RSM). Also, the nano-synthesis and preparation of STF were examined using rheometric tests. The possibility of STFs with various initial viscosity compositions was investigated. The following are some critical findings:

(i) According to RSM data, the optimal complex viscosity may be obtained with a percentage of STF with oil of 0.4 and an applied force of 90 kN at a loading frequency of 1.44 Hz. When using RSM's proposed regression model, the experimental values correspond well with the projected values. According to the ANOVA, the percentage of STF with oil has a substantial impact on the complex viscosity.

(ii) An excessively high or low load frequency restricts the damping constant and effective stiffness, which would improve joint strength and bolt life. The maximum damping constant under ideal conditions is 446.99 N.s/mm, with a desirability of 0.971. For future work, the created model can be utilised to estimate the effective composition of nano-silica with PEG.

(iii) Because of particle agglomeration, the damping constant of nano-silica may decrease due to an increase in particle size and changes in the pore structure.

(iv) Nonetheless, the limited sequestration capacity of STF obtained from the type of nano-additives

remains a significant potential to rigorous technical, economic, and feasibility study that has been proposed for future exploration in order to fully exploit the STF's dampening capabilities.

Abbreviations

STF: Shear thickening fluid
RSM: Response surface method
PEG: Polyethylene glycol.

Data Availability

The data used to support the findings of the study are included within the article.

Conflicts of Interest

The authors declare that they have no conflicts of interest.

Authors' Contributions

Ruby Freya conceived the conceptual ideas and performed the analysis and experimental work. R. Senthil collected and contributed the data for analysis, wrote the original manuscript, and supervised the study completely.

References

[1] M. K. Prajapati and S. Jamle, "Strength irregularities in multistoried building using base isolation and damper in high Seismic zone: a theoretical Review," *International Journal of Advanced Engineering Research and Science (IJAERS)*, vol. 7, no. 3, pp. 235–238, 2020.

[2] J. Qureshi, Y. Nadir, and S. K. John, "Bolted and bonded FRP beam-column joints with semi-rigid end conditions," *Composite Structures*, vol. 247, Article ID 112500, 2020.

[3] A. Daniūnas and K. . Urbonas, "Analysis of the steel frames with the semi- rigid beam-to-beam and beam-to-column knee joints under bending and axial forces," *Engineering Structures*, vol. 30, no. 11, pp. 3114–3118, 2008.

[4] G. Zhang, Q. Fan, Z. Lu, Z. Zhao, and Z. Sun, "Experimental and numerical study on the seismic performance of rocking steel frames with different joints under earthquake excitation," *Engineering Structures*, vol. 220, Article ID 110974, 2020.

[5] A. Ghabussi, J. Asgari Marnani, and M. S. Rohanimanesh, "Improving seismic performance of portal frame structures with steel curved dampers," *Structures*, vol. 24, pp. 27–40, 2020.

[6] H. Fang, X. Meng, L. Duan, Y. Liu, and H. Jin, "Advanced steel brace with multistable hysteretic damping enhanced by a multilayered structure," *Marine Structures*, vol. 73, Article ID 102800, 2020.

[7] A. Köken and M. A. Köroğlu, "Experimental study on beam-to-column connections of steel frame structures with steel slit dampers," *Journal of Performance of Constructed Facilities*, vol. 29, no. 2, Article ID 0000553, 2015.

[8] G. W. Rodgers, J. B. Mander, and J. G. Chase, "Experimental testing and analytical modelling of damage-avoidance steel connections using HF2V damping devices," in *Proceedings of the 2009 NZSEE Conference*, pp. 1–8, Christchurch, New Zealand, April 2009.

[9] I. Takewaki and H. Akehashi, "Comprehensive review of optimal and smart design of nonlinear building structures with and without passive dampers subjected to earthquake loading," *Frontiers in Built Environment*, vol. 7, Article ID 631114, 2021.

[10] K. Ghaedi, "Earthquake prediction," *Earthquakes - Tectonics, Hazard and Risk Mitigation*, vol. 66, pp. 205–227, 2017.

[11] C. Abarkane, G. Ríos-García, D. Gale-Lamuela, F. Rescalvo, A. Gallego, and A. Benavent-Climent, "Metallic slit-plate dampers: damage evaluation with metal magnetic memory technique and application to structures with rocking columns," *Metals*, vol. 9, no. 9, p. 953, 2019.

[12] H. Akehashi and I. Takewaki, "Resilience evaluation of elastic-plastichigh-rise buildings under resonant long-duration ground motion," *Japan Architectural Review*, vol. 5, no. 4, pp. 373–385, 2022.

[13] E. Islam, G. Kaur, D. Bhattacharjee, S. Singh, I. Biswas, and S. K. Verma, "Effect of cellulose beads on shear-thickening behavior in concentrated polymer dispersions," *Colloid and Polymer Science*, vol. 296, no. 5, pp. 883–893, 2018.

[14] N. Y. C. Lin, C. Ness, M. E. Cates, J. Sun, and I. Cohen, "Tunable shear thickening in suspensions," *Proceedings of the National Academy of Sciences*, vol. 113, no. 39, pp. 10774–10778, 2016.

[15] K. Lin, H. Liu, M. Wei, A. Zhou, and F. Bu, "Dynamic performance of shear-thickening fluid damper under long-term cyclic loads," *Smart Materials and Structures*, vol. 28, no. 2, Article ID 025007, 2018.

[16] A. Ras and N. Boumechra, "Study of nonlinear fluid viscous dampers behaviour in seismic steel structures design," *Arabian Journal for Science and Engineering*, vol. 39, no. 12, pp. 8635–8648, 2014.

[17] M. Wei, K. Lin, Q. Guo, and H. Sun, "Characterization and performance analysis of a shear thickening fluid damper," *Measurement and Control*, vol. 52, no. 1-2, pp. 72–80, 2019.

[18] M. Wei, K. Lin, and H. Liu, "Experimental investigation on hysteretic behavior of a shear thickening fluid damper," *Structural Control and Health Monitoring*, vol. 26, no. 9, p. 2389, 2019.

[19] X. Z. Zhang, W. H. Li, and X. L. Gong, "The rheology of shear thickening fluid (STF) and the dynamic performance of an STF-filled damper," *Smart Materials and Structures*, vol. 17, no. 3, Article ID 035027, 2008.

[20] H. Zhou, L. Yan, W. Jiang, S. Xuan, and X. Gong, "Shear thickening fluid–based energy-free damper: design and dynamic characteristics," *Journal of Intelligent Material Systems and Structures*, vol. 27, no. 2, pp. 208–220, 2014.